UNITED STATES DEPARTMENT OF THE INTERIOR

GEOLOGICAL SURVEY

Colored Gravity Anomaly and Terrain Maps of the Northeastern U.S. and Adjacent Canada

by

R. W. Simpson, W. A. Bothner and R. H. Godson

Open-File Report 81-560

1981

Open-File Report 81-560

Avalible with 5" x 7" color xeroxes of the maps or with standard 2" x 2" color Slides.

The colord xeroxes will be substantially cheaper, but the quality of the originals is degraded to such a degree that the xerox copies are only marginally usable.

The Color slides can be purchased through:

US Geological Survey
The Denver Photo Library
Mail Stop 914
Denver CO 80225

Colored Gravity Anomaly and Terrain Maps of the Northeastern U.S. and Adjacent Canada

by

R. W. Simpson, W. A. Bothner and R. H. Godson

INTRODUCTION

As a part of the Earthquake Hazards and Reactor Hazards Programs for the northeastern United States, we have compiled and plotted the available gravity and terrain data on a regional scale. Reproductions of colored maps displaying this data are available with this report either as 5" x 7" color Xeroxes or as 2" x 2" colored slides. These maps reveal many interesting regional patterns which help to provide a perspective for more detailed local studies.

The distribution of gravity anomalies, when compared with the patterns of seismicity, also provides some clues as to the origin of intraplate earthquakes in the northeast. We note, for example, that earthquakes do not seem to occur very frequently in areas with low gravity gradients, while areas with moderate to high amplitude residual anomalies sometimes (though not always) have concentrations of seismicity nearby. There is a hint that regions with a NE grain to the residual anomalies experience more earthquakes than areas with other or random trends. Many of the gravity anomalies and gradients which do correlate with seismicity mark old structures and zones of weakness. This observation is consistent with the world-wide correlations of intraplate seismicity and pre-existing zones of weakness documented by Sykes (1978).

THE DATA SETS

1. Gravity Data

The gravity data used in the preparation of these maps is described in more detail in Bothner and others (1980). It consists of approximately 100,000 stations obtained from the Defense Mapping Agency (DMA), from the National Oceanic and Atmospheric Administration (NOAA) Data Center, from the Canadian Gravity Data Centre, and from many workers who kindly furnished us with gravity stations not listed in the larger catalogs. All new data have been submitted to the DMA for inclusion in their master file and will eventually be available through the NOAA Data Center.

The U.S. on-land gravity stations have been computer terrain corrected from 167 km into a distance of 0.895 km from the station using a program of Plouff (1977). We believe the inner zone corrections, which we have omitted, to be insignificant for probably 99 percent of the stations. That is, the inner corrections are expected to be substantially less than the 2 milligal uncertainty which we estimate for the majority of the land observations. Some mountainous areas do have inner zone corrections in excess of 2 milligals, but we do not expect that our neglect of these corrections will change the regional anomaly patterns in any significant way at this scale.

In spite of much editing, some bad data points are still apparent--especially in the gradient plots where they produce small four-petal flower patterns. Questions about single small anomalies should be referred to larger scale maps and to the original published maps where these are available. The marine data present especially severe editing problems and the estimated error for marine stations varies to as large as 5 to 10 milligals. Many of the higher frequency anomalies in the oceanic and lake areas reflect this inaccuracy as well as offsets in gravity values at the crossings of separate profile tracks. These incompatabilities become especially apparent in the derivative and gradient maps where high frequencies are being emphasized, producing some highly colored small wavelength anomalies.

The data set was first screened at a 5 km interval by selecting only one station per 5 km x 5 km cell where data were available. This reduced the number of stations used to approximately 45,000. The choice of a 5 km cell size was a compromise between using as much data as possible, and yet not biasing the final display by wide variations in data density. Figures 1, 2, and 3 show the data density at cell sizes of 2.5 km, 5.0 km, and 7.5 km.

A minimum curvature algorithm (Briggs, 1974) programmed by Webring (1977), was then used to do the necessary interpolation and extrapolation to produce a rectangular grid of values with 5 km interval between grid points.

The original grid was approximately 70 km larger on all sides, but was trimmed to the present size in order to reduce edge effects. Possible edge effects still appear on certain of the maps in the form of high or low anomalies paralleling the edges of the map, however, and the user should be aware of this problem.

The final step was to regrid (using a splining algorithm) the basic 5 km grid to a finer 2.032 km grid size so as to be compatible with the pixel size required by the Applicon Color Plotter. White areas on the map indicate that there were no data points within 10 km of the grid point.

The data were projected using the Albers Conic Equal-Area projection with standard parallels for the U.S. (29.5°N, 45.5°N), so that the maps are compatible with the U.S. Geologic Map.

2. Terrain Data

Terrain data were obtained from the National Geodetic Survey (NGS) who in turn received it from the Electromagnetic Compatability Analysis Center (ECAC), an agency of the Department of Defense (DoD). The data were extensively edited and reformatted (by R. H. Godson) to produce average elevations for the entire country at 30", 1', and 3' intervals. This data set has been submitted to the NOAA Data Center (National Geophysical and Solar-Terrestrial Data Center, National Oceanic and Admospheric Administrtion, Boulder, CO 80303) for distribution.

DESCRIPTION OF THE MAPS

1. Free Air Gravity

This map displays the free air anomaly field calculated using the 1967 Geodetic Reference System formula for theoretical gravity (International Association of Geodesy, 1971). Observed gravity values have been adjusted to conform to the International Gravity Standardization Net of 1971 (Morelli, 1974).

2. Bouguer Gravity

Bouguer anomalies were also calculated using the new geodetic reference system (see references above) and a reduction density of 2.67 g/cm^3. Land stations in the U.S. have been computer terrain corrected into a distance of 0.895 km from the station. Estimated error on most land stations is less than about 1/2 of a 5 milligal color interval. Marine stations may be in error by as much as 10 milligals.

3. Bouguer Residual (250 km)

Using a Fourier transform filtering program written by Hildenbrand (1979), wavelengths greater than 250 km in the Bouguer anomaly field were suppressed. (A ramped high pass filter was used with a ramp betwen 200 km and 300 km.) This has the effect of removing a regional field consisting of the broader features of the gravity field. The extracted regional is displayed in Figure 4.

The high amplitude (red) anomalies along the left edge near the bottom and along the top edge at the right are enhanced by edge effects which have not been completely removed by the trimming process described above. These edge effects result from Fourier transforming the Bouguer gravity field with its very high oceanic values in the lower right corner of the map, since the fast Fourier transform algorithm assumes that the finite rectangular grid is infinitely periodic in both the x and y directions.

Wavelength filtering also tends to produce spurious anomalies flanking real anomalies (Ulyrch, 1968). A linear high will be flanked by two lower amplitude parallel lows outboard of which will be two parallel highs (of very much smaller amplitude than the original). This tends to give the map a grain roughly equal in wavelength to the cut of the filter. Thus all anomalies must be interpreted with care. The dangers, we feel, are more than compensated for by the enhancement of many structures and features of geologic interest. For example, the boundary between the Grenville and Superior Precambrian provinces which cuts diagonally across the northwest corner of the map is very clearly marked by a change in the amplitude and trend of the residual anomalies.

4. Bouguer Residual (100 km)

This map is similar to the previous map except that now wavelengths greater than 100 km have been suppressed. (A ramped high pass filter with a ramp from 80 to 120 km was used.) The extracted regional is displayed in Figure 5. Anomalies produced by a point source at 33 km depth have a half-width of 50 km (this is about $\frac{1}{2}$ of a wavelength). Thus most of the anomalies displayed in the 100 km residual map will be produced by sources at depth less than about 33 km. Note, however, that not all the anomalies produced by near-surface sources have escaped the filtering; broader anomalies produced by facies changes or the gradual feathering of density contrasts over distances greater than 100 km will also be suppressed, even though the density contrast may be very near the surface.

A 100 km anomaly grain produced by the wavelength filtering is quite obvious in this map. The same caution in interpreting anomalies mentioned for the 250 km residual map applies here. The reality of features of interest can often be verified by comparing with the second vertical derivative which is a smoother form of high pass filtering which does not introduce an anomaly grain at the cutoff wavelength.

Areas with low amplitude residual anomalies seem in general to have fewer earthquakes. Not all areas with high amplitude anomalies have concentrations of earthquakes, though areas with northeast trending residual anomalies seem more prone to seismicity than areas with other trends. This suggests that perhaps old northeast-trending structures are being reactivated in a regional EW compressive stress field (Zoback and Zoback, 1980).

Of particular interest to earthquake studies are the three segments of NNE trending highs and lows connecting the Attica, N.Y. area with the Cornwell, Ontario-Massena, N.Y. area. Both these regions are separate loci of epicenters (Hadley and Devine, 1974). The gravity data suggest that both lie on segments of an old structure--perhaps a graben offset by E-W transforms or strike-slip dislocations.

5. Second Vertical Derivative of Bouguer Anomalies

The second vertical derivative of the Bouguer anomaly field was calculated using Hildenbrand's Fourier transform filtering program. The effect of this filter is to multiply the various wavelength components of the Bouguer Field by $(1/\text{wavelength})^2$ which greatly enhances the shorter wavelengths and, hence, the near-surface density contrasts. The zero level of the second vertical derivative marks the steepest gradients of anomalies and is frequently taken as a good indicator of the position of density boundaries and the horizontal extent of geologic bodies.

Because this filter greatly enhances the high frequencies--including those produced by bad data points--the data were initially upward continued to an elevation of 5 km before applying the second derivative filter in order to reduce some of the irregularities in the data. This step is a compromise between noise and resolution.

6. Horizontal Gradient of the Bouguer Gravity

The magnitude of the horizontal gradient of the Bouguer anomaly field was calculated using the basic equation:

$$\left|\text{gradient}\right| = \sqrt{\left(\frac{\partial z}{\partial x}\right)^2 + \left(\frac{\partial z}{\partial y}\right)^2}$$

and the approximations that

$$\left(\frac{\partial z}{\partial x}\right)_{i,j} = \frac{z_{i+1,j} - z_{i-1,j}}{2(\Delta x)}, \text{ and } \left(\frac{\partial z}{\partial y}\right)_{i,j} = \frac{z_{i,j+1} - z_{i,j-1}}{2(\Delta y)}$$

This approximation can be shown to be equivalent to fitting a parabola at grid point i using z_i and its 2 neighboring values z_{i+1}, z_{i-1} and then calculating the slope of the parabola at i. The magnitude of the gradient of an anomaly depends on both the size of the density contrast and the nearness of the source to the surface. The largest gradients will often occur nearly over the mass contrast at the edges of geologic bodies. Cordell (1979) has used the

horizontal gradient to locate faults. Note, however, that the steepest gradients produced by an ideal point source at depth or an equivalent spherical source may have nothing to do with the physical extent of the body.

Horizontal gradients produced by linear anomalies are steepest over the two sides and gentle or flat along the tops of the anomalies so that there are two flanking high gradients and a medial low gradient. Nearly circular anomalies have their highest gradients circling them. The result on the color map is a red doughnut encircling the anomaly.

Many of the straighter gradients mark structural boundaries of plate tectonic origin. The N-S gradient through Vermont and western Massachusetts seems to mark a density contrast which was produced by thrusting associated with the collision of an island arc with the North American craton in Ordovician time. Other linear gradients to the east, though not as well defined as the one through Vermont, support the idea that the Appalachians were produced by a number accretional events involving the collisions of island arcs, micro-continents and ultimately another continent.

Many of the circular and highly curved gradients mark the mapped contacts of felsic and mafic plutons, suggesting that other similar gradients showing no correspondence with surface geology mark buried plutons.

7. Horizontal Gradient of Bouguer Gravity with Earthquakes

McGinnis and Ervin (1974), Long (1976), Forsyth (1977) ,and Simmons and others (1978) have pointed out apparent correlations of earthquakes with the gradient of the Bouguer gravity field. This slide shows a plot of all earthquakes in the U.S.G.S. catalog for the Northeastern United States. Although many earthquakes lie in areas with high gradients, there are also many large gradients which do not show signs of seismicity.

Perhaps the gradients with little associated seismicity mark structures which are not being reactivated since they are not favorably oriented with respect to the regional stress field. Another possibility is that our earthquake record is not long enough to establish the true patterns of seismicity.

It does appear that areas with low gravity gradient have fewer earthquakes. This may reflect a smaller number of major structures in these areas, but it is also possible that the lower gradients reflect a greater depth to the Precambrian basement which contains the structures under a thick cover of Paleozoic sedimentary rocks. If the Precambrian basement is deeper, it may be in a rheological regime where creep or plastic deformation is more likely to occur than brittle, earthquake-producing fracture.

8. Load Induced Stress Difference at 7.5 km

Topographic features and masses producing short wavelength anomalies must be supported to some extent by stresses in the crust (McNutt, 1980). To obtain an estimate of the magnitude and distribution of these stresses, the free air anomaly was converted to an equivalent two-dimensional density distribution which was then distributed over the free surface of a semi-infinite elastic half-space. If the rather small terrain corrections for this region are ignored, this is equivalent to loading an elastic half-space with a surface load determined by the mass of the topographic features and then adding a second surface load determined as the equivalent two-dimensional surface mass distribution which would produce the observed Bouguer anomalies. (Any gravity anomaly field can be accounted for in terms of a fictional "equivalent source" or "density coating" distributed over a flat surface of observation (Grant and West, 1965, p. 214).)

The density contrasts, as represented by the equivalent surface sources, are more smeared than the actual sources at depth so that the stresses calculated will necessarily be more distributed and less concentrated than those actually occurring. Loading all crustal mass anomalies at the surface rather than at their true depths also has the effect of increasing the stresses near the surface, but decreasing them at the depths at which the true sources lie. Both these effects will therefore tend to underestimate the load induced stresses at depth. However, for a first approximation, the computational simplicity of this approach has much to recommend it.

Another problem is that the elastic half-space assumption is a good approximation only for wavelengths shorter than the thickness of the Earth's elastic layer--for wavelengths longer than this thickness, a more appropriate model would be an elastic layer over a plastic half-space of appropriate rheology. To avoid artifacts produced by long wavelength anomalies which are outside the domain of the simple elastic half-space model, the free air anomalies were high pass filtered with a cutoff at 100 km so that only the shorter wavelengths of the free air field were used.

The surface load, inferred from the free air anomaly field, was then Fourier transformed to resolve its contribution into discrete wavelengths. The solution for a doubly sinusoidal load on an elastic half-space (Fung, 1965, p. 195) allows the stress tensor at any depth to be found by calculating the contribution from each separate wavelength and summing (doing the inverse Fourier transform).

The stress difference plotted in the color map is the difference between the largest and smallest eigenvalues of the stress tensor calculated at a depth of 7.5 km. The stress difference serves as a crude measure of how close the homogeneous elastic material is to failure. It is our feeling that the stresses are, if anything, underestimated because of the various assumptions made.

In attempting to correlate the load induced stress difference with earthquake occurrence, another important variable is the mechanical heterogeneity of the crust. Although stresses presumably cause earthquakes, the vastly different strengths of various rock types under various conditions of pressure and temperature may be at least as important as the concentration of large stresses in localizing earthquakes. In fact, the load induced stresses as calculated by this method correlate poorly with the general pattern of seismicity. Certain areas such as Anna, Ohio and the lower St. Lawrence Valley area in Canada have large load induced stresses near areas of seismicity. The load induced stresses in these areas may well contribute to other stresses to localize seismicity (Goodacre and Hasegawa, 1980), but in general load induced stresses do not seem to be a primary cause of seismicity.

9. Terrain

The elevation data at 1' intervals were used to prepare this grid. The data were projected (Albers) and regridded to 2.032 km intervals to produce a map at a scale of 1:2,500,000 on the color plotter.

Barosh (1978) has pointed out a correlation of seismicity with lowland areas and river valleys in large parts of the northeast.

10. Terrain Slope

The same process used to calculate the horizontal gradient of the Bouguer anomaly field was used to calculate the terrain slope.

REFERENCES CITED

Barosh, P. J., 1978, Earthquakes and faults in the Northeastern United States: Geological Society of America, Abstracts with programs, v. 10, n. 2, p. 32.

Bothner, W. A., Simpson, R. W., and Diment, W. H., 1980, Bouguer gravity map of the Northeastern United States and adjacent Canada: U.S. Geological Survey Open-File Report 80-2012, scale 1:1,000,000.

Briggs, I. C., 1974, Machine contouring using minimum curvature: Geophysics, v. 39, p. 39-48.

Cordell, Lindrith, 1979, Gravimetric expression of graben faulting in Santa Fe Country and the Espanola Basin, New Mexico: New Mexico Geol. Soc. Guidebook, 30th Field Conf., Santa Fe Country, p. 59-64.

Forsyth, D. A., 1977, Reltionships between seismicity, free air gravity and structure in Arctic and eatern Canada (abs.): Earthquake Notes, v. 48, p. 15.

Fung, Y. C., 1965, Foundations of Solid Mechanics, Prentice Hall, Englewood Cliffs, N.J.

Goodacre, A. K. and Hasegawa, H. S., 1980, Gravitationally induced stresses at structural boundaries: Canadian Journal of Earth Sciences, v. 17, p. 1286-1291.

Grant, F. S., and West, G. F., 1965, Interpretation theory in applied geophysics: McGraw-Hill Book Company, N.Y., 584 p.

Hildenbrand, T. G., 1979, Preliminary documentation of program FFTFIL: U.S. Geological Survey, unpublished documentation.

International Association of Geodesy, 1971, Geodetic Reference System 1967: International Association of Geodesy Special Publication, no. 3, 116 p.

Long, L. T., 1976, Speculations concerning Southeastern earthquakes, mafic intrusions, gravity anomalies, and stress amplification: Earthquake Notes, v. 47, p. 29-35.

McGinnis, L. D., and Ervin, C. P., 1974, Earthquakes and block tectonics in the Illinois Basin: Geology, v. 2, p. 517-519.

McNutt, Marcia, 1980, Implications of regional gravity for state of stress in the Earth's crust and upper mantle: Journal of Geophysical Research, v. 85, p. 6377-6396.

Morelli, C., (ed.), 1974, The International Gravity Standardization Net 1971: International Association of Geodesy Special Publication, no. 4, 194 p.

Plouff, D., 1977, Preliminary documentation for a FORTRAN program to compute gravity terrain corrections based on topography digitized on a geographic grid: U.S. Geological Survey Open-File Report 77-534, 45 p.

Simmons, G., Tillson, D., Murphy, V., LeBlanc, G., Doherty, J., Sharp, J., and Roeloff, E., 1978, Gravity, stress, and earthquakes in Washington State and surrounding areas (abs.): 3rd International Conference on Basement Tectonics, 15-19 May 1978, Fort Lewis College, Durango, CO.

Sykes, L. R., 1978, Intraplate seismicity, reactivation of preexisting zones of weakness, alkaline magmatism, and other tectonism postdating continental fragmentation: Reviews of Geophysics and Space Physics, v. 16, p. 621.

Ulyrch, T. J., 1968, Effect of wavelength filtering on the shape of the residual anomaly: Geophysics, v. 33, p. 1015-1018.

Webring, M. W., 1977, Preliminary documentation--gridding program MINC: U.S. Geological Survey, unpublished documentation.

Zoback, M. L., and Zoback, M. D., 1980, State of stress in the conterminous United States: Journal of Geophysical Research, v. 85, p. 6113-6156.

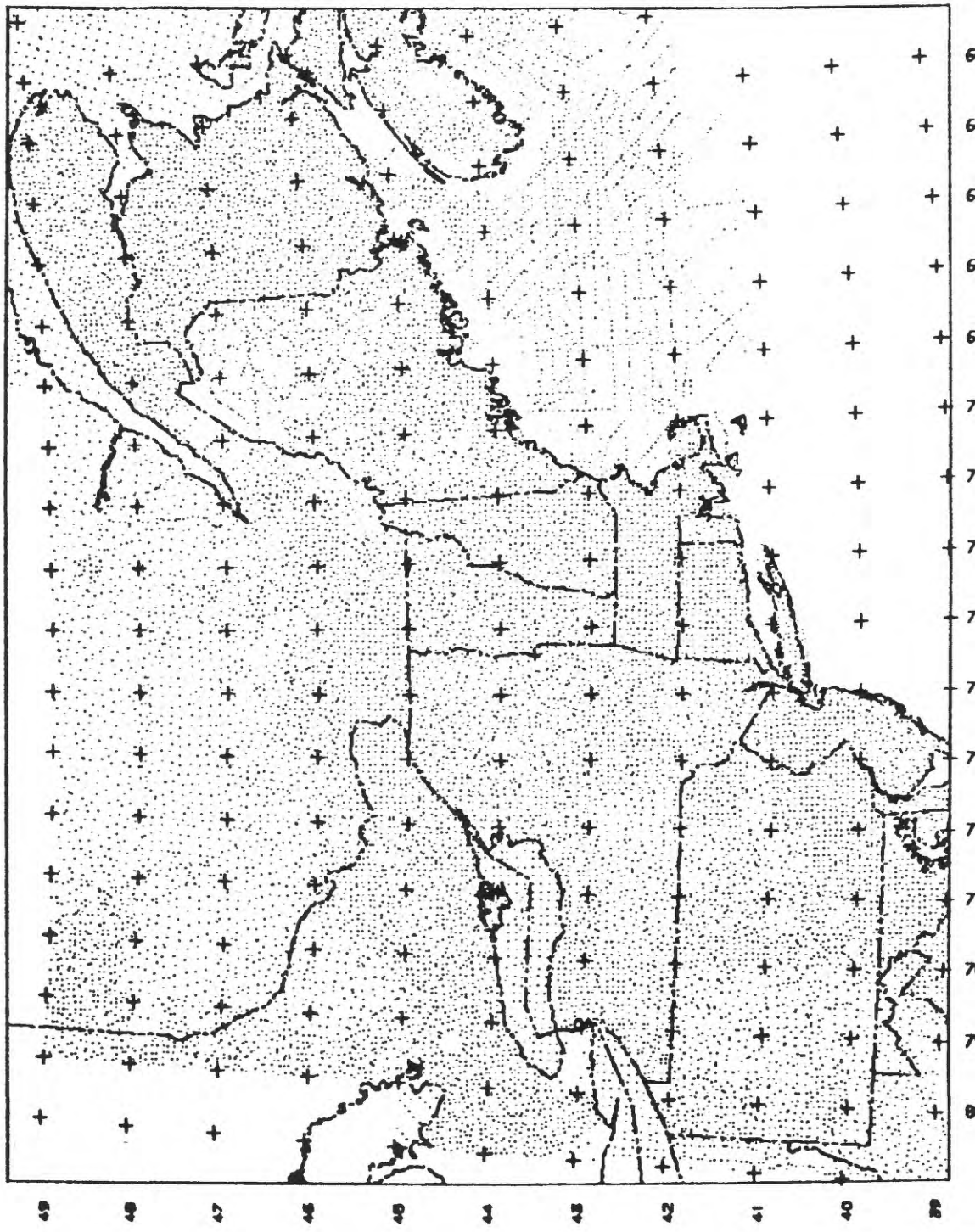

Figure 3. Data set screened at 7.5 km cell size.

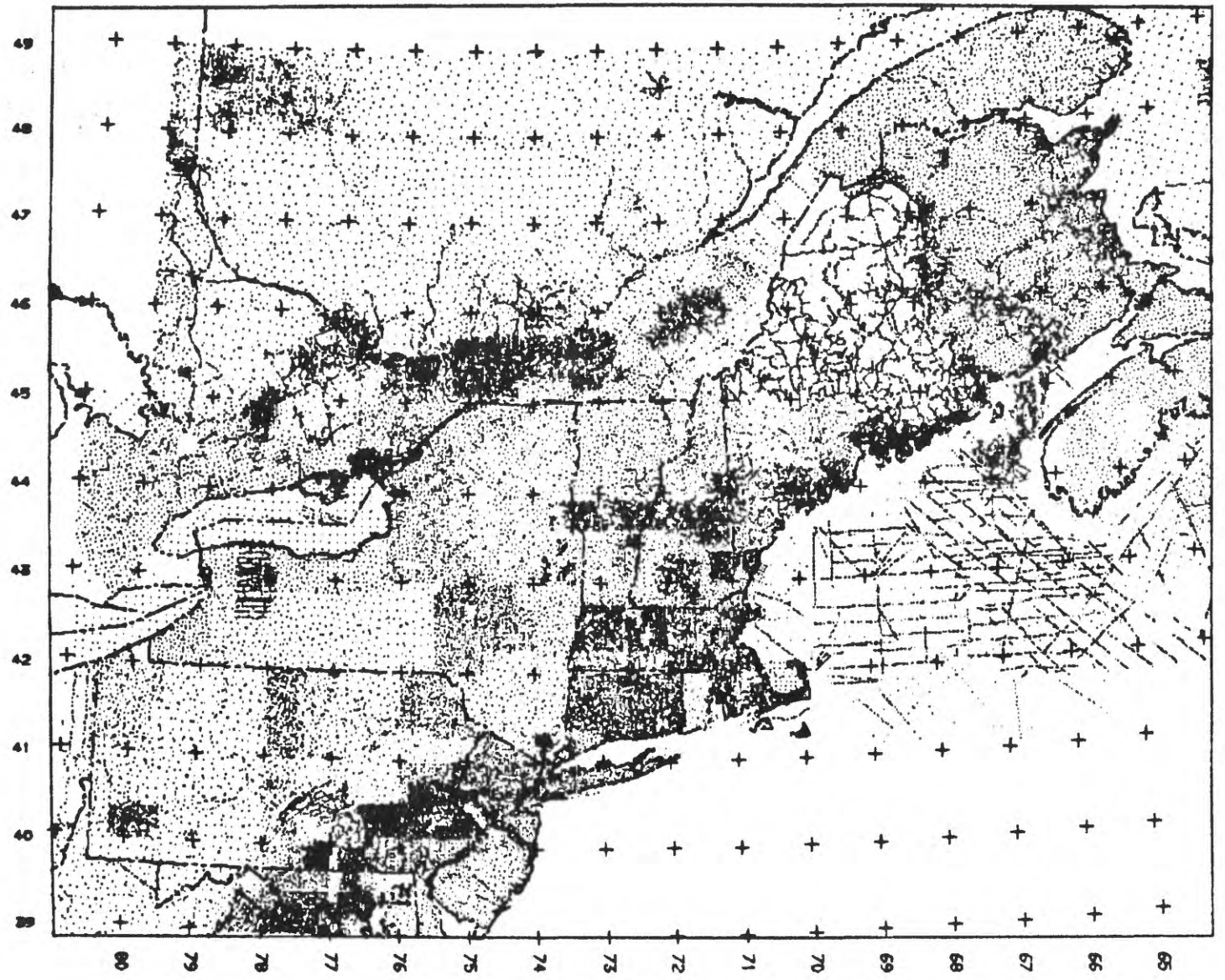

Figure 1. Data set screened at 2.5 km cell size.

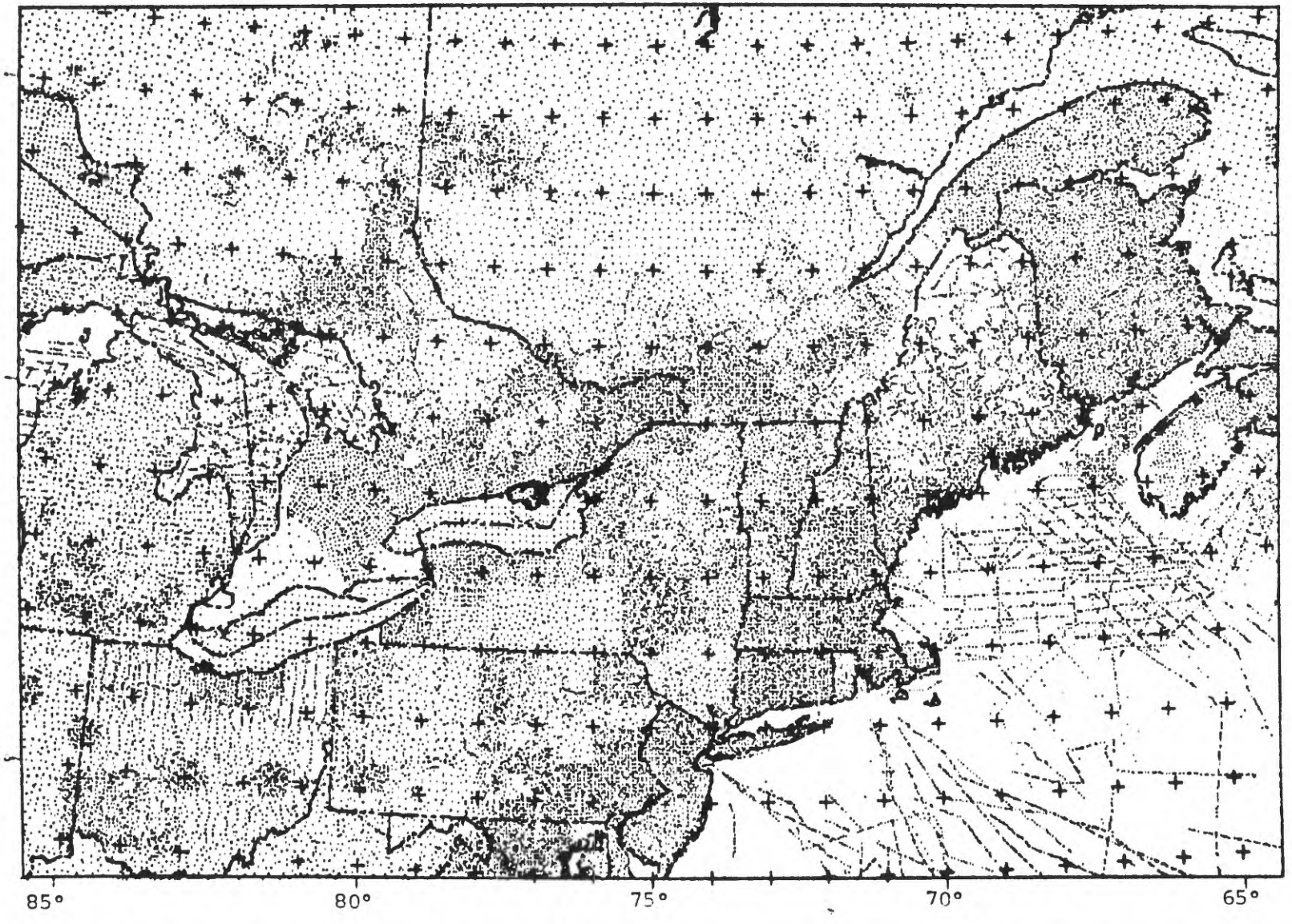

Figure 2. Data set screened at 5.0 km cell size. This set was used to prepare color maps.

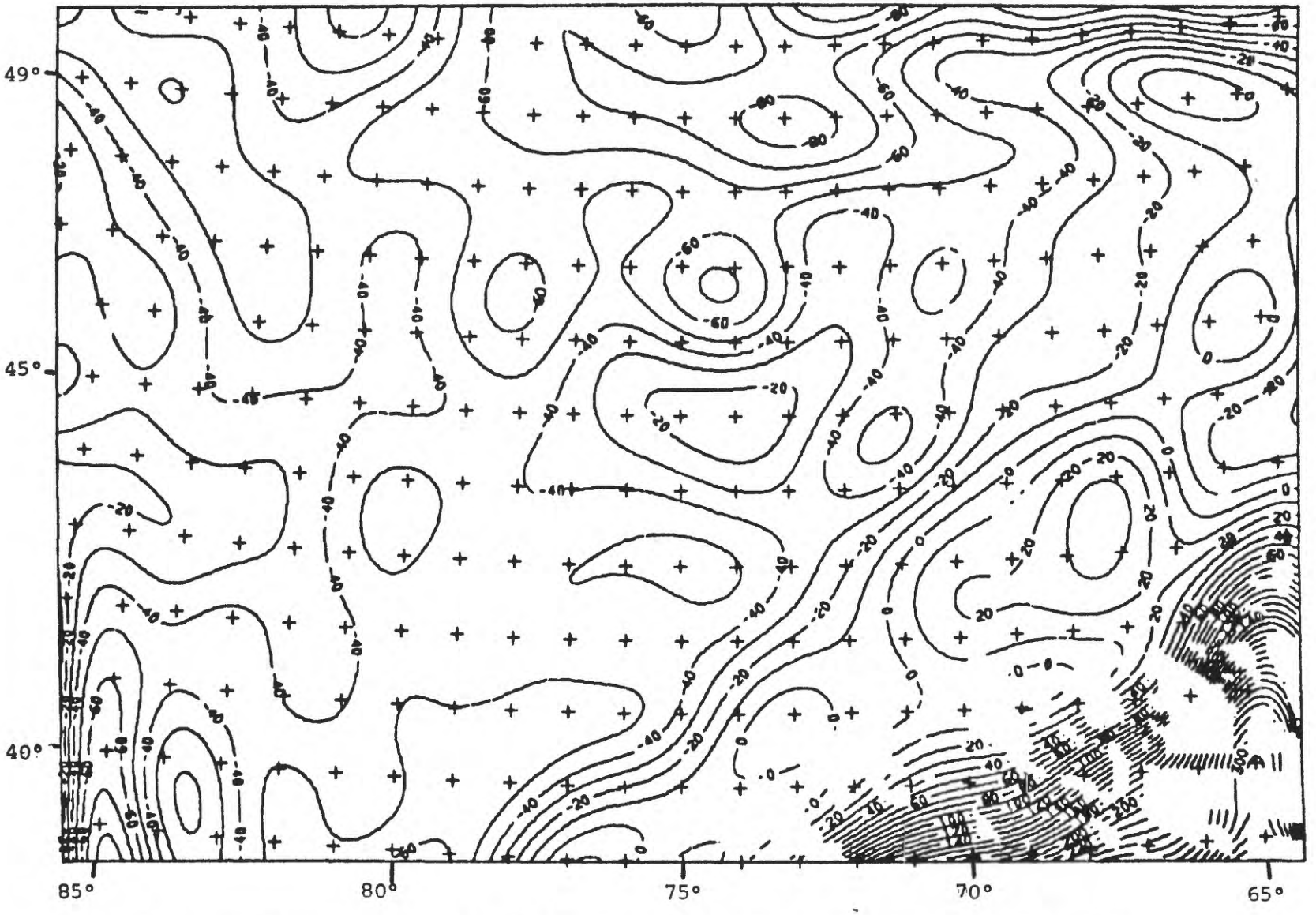

Figure 4. Regional Bouguer anomaly field composed of wavelengths greater than 250 km.

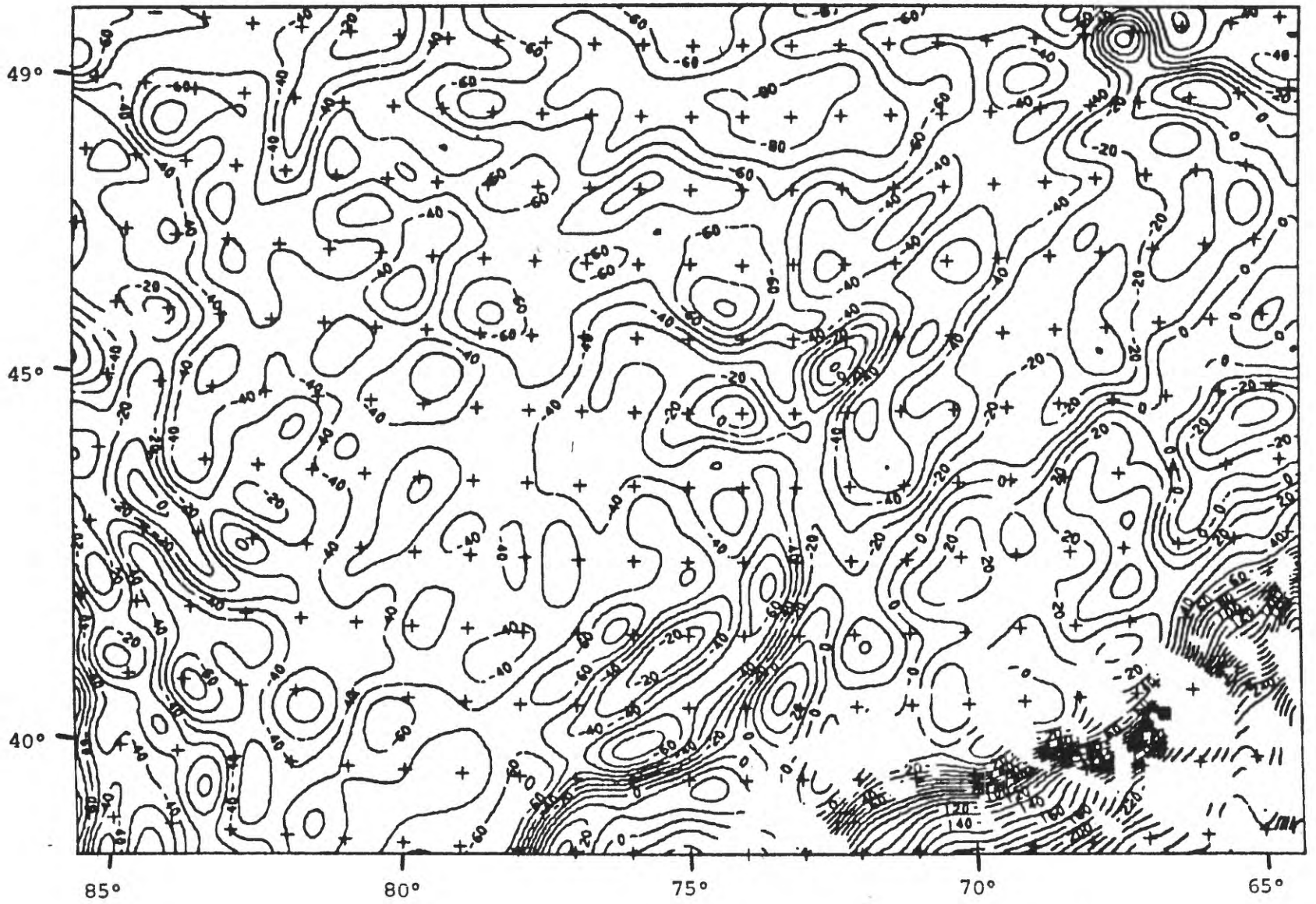

Figure 5. Regional Bouguer anomaly field composed of wavelengths greater than 100 km.

MAP 1. Free Air Gravity (range = -60 to +50 milligals)

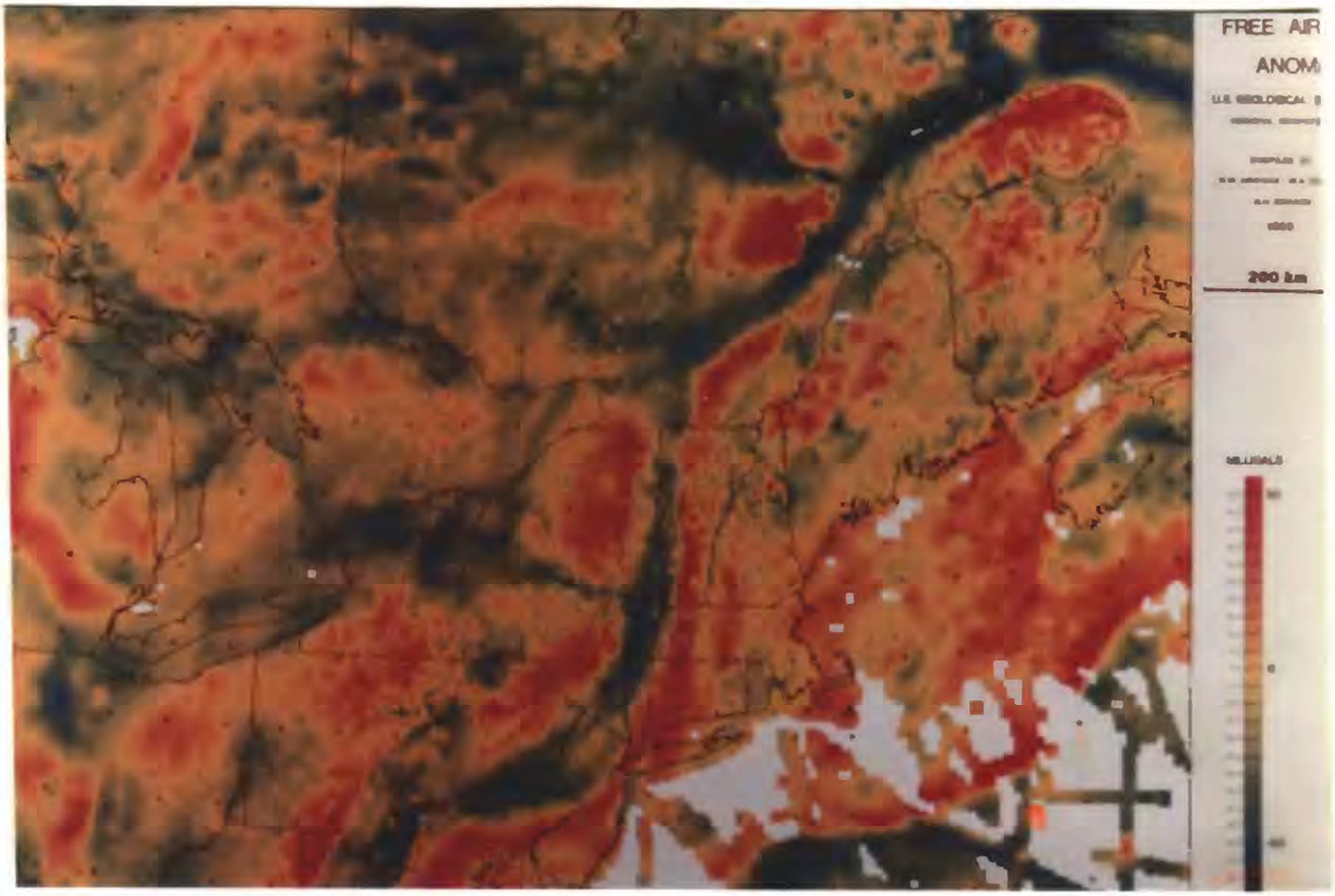

MAP 2. Bouguer Gravity (range = -95 to +55 milligals)

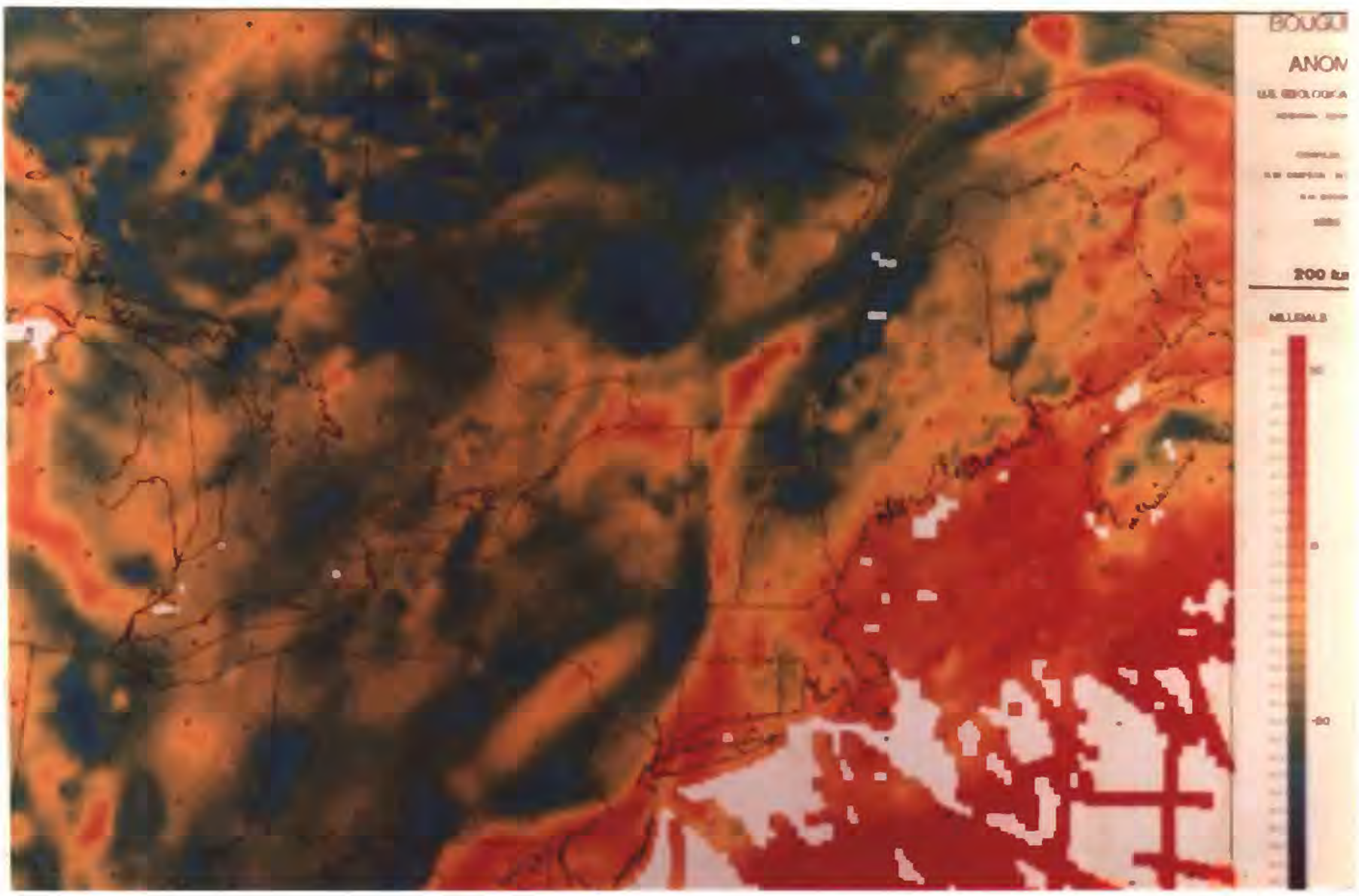

MAP 3. Bouguer Residual, 250km (range = -30 to +30 milligals)

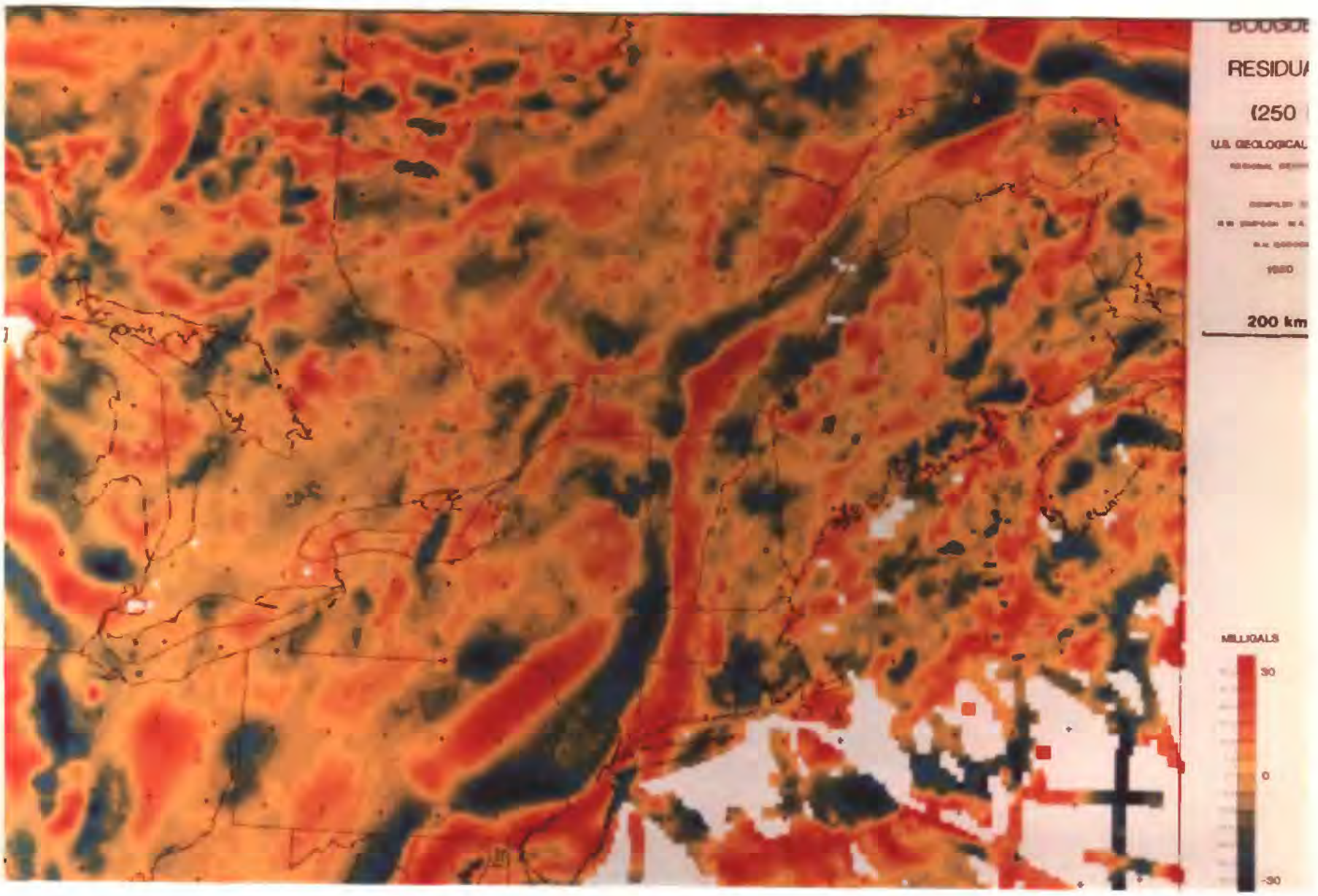

MAP 4. Bouguer Residual, 100km (range = -30 to +30 milligals)

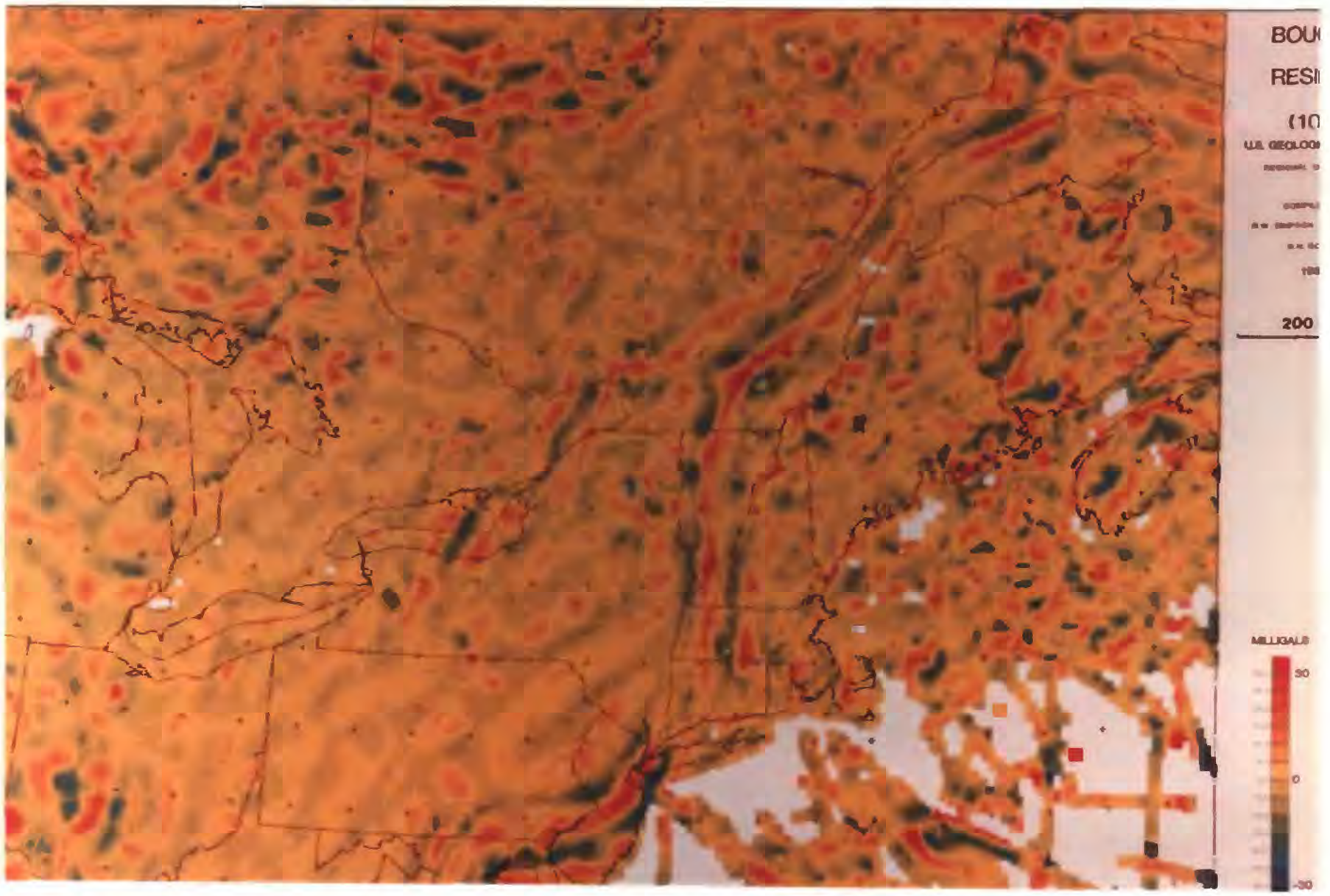

MAP 1. Free Air Gravity (range = -60 to +50 milligals)

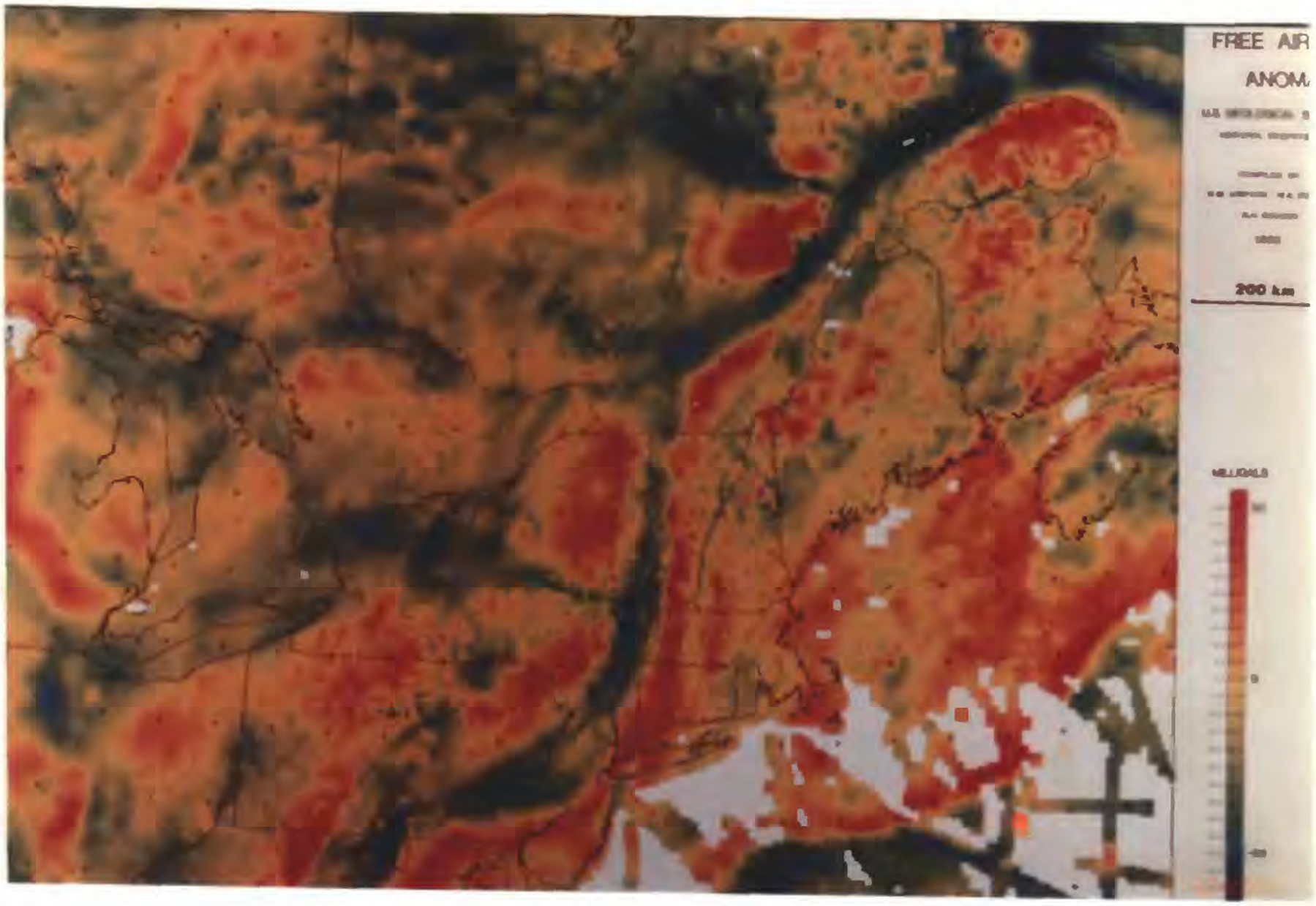

MAP 2. Bouguer Gravity (range = -95 to +55 milligals)

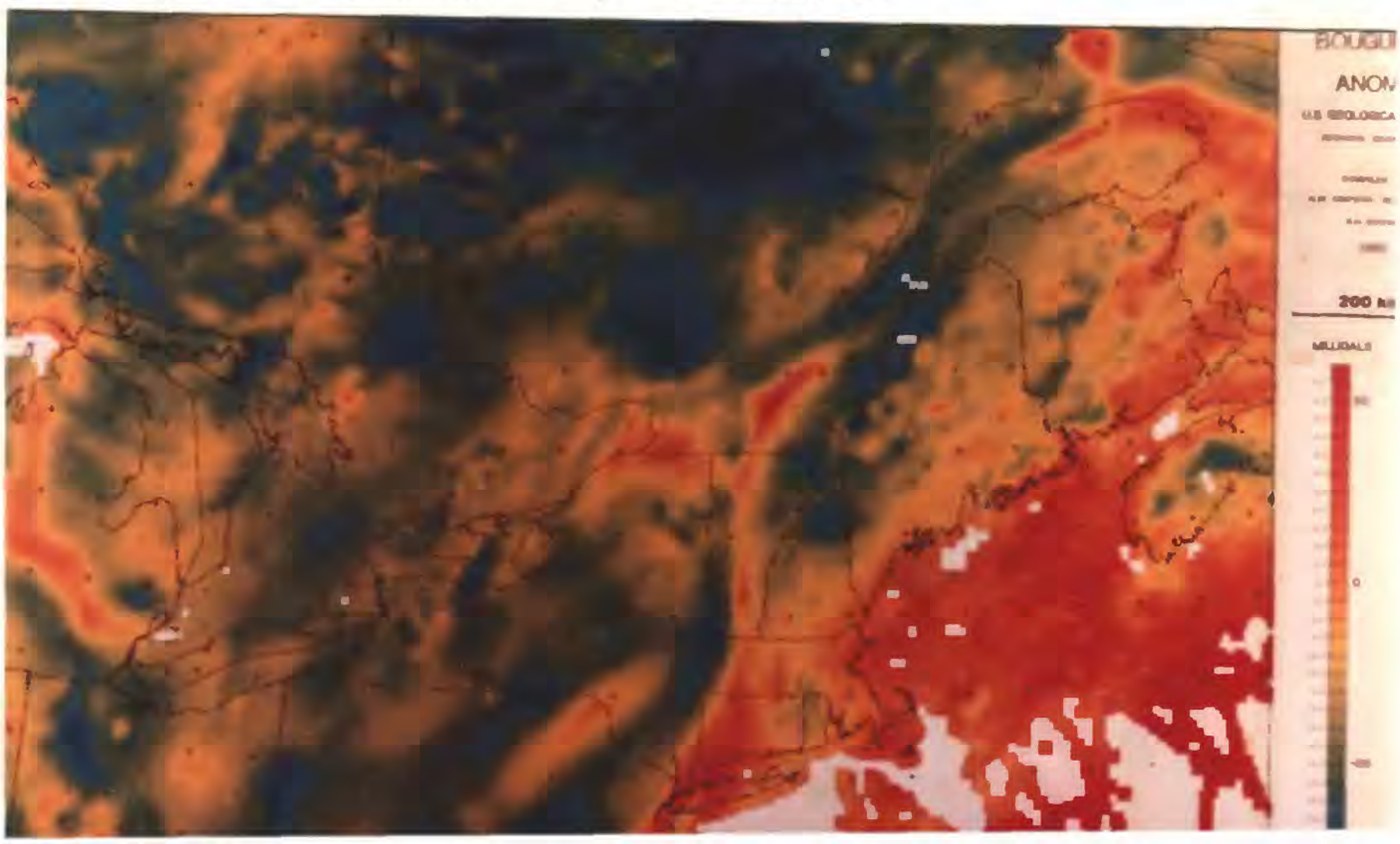

MAP 5. Second Vertical Derivative (range = -0.3 to +0.3 milligals/km^2)

MAP 6. Horizontal Gradient of Bouguer Gravity (0 to 2.5 milligals/km)

MAP 7. Horizontal Gradient with Earthquakes (0 to 2.5 milligals/km)

MAP 8. Load Induced Stress Difference at 7.5km (0 to 50 bars)

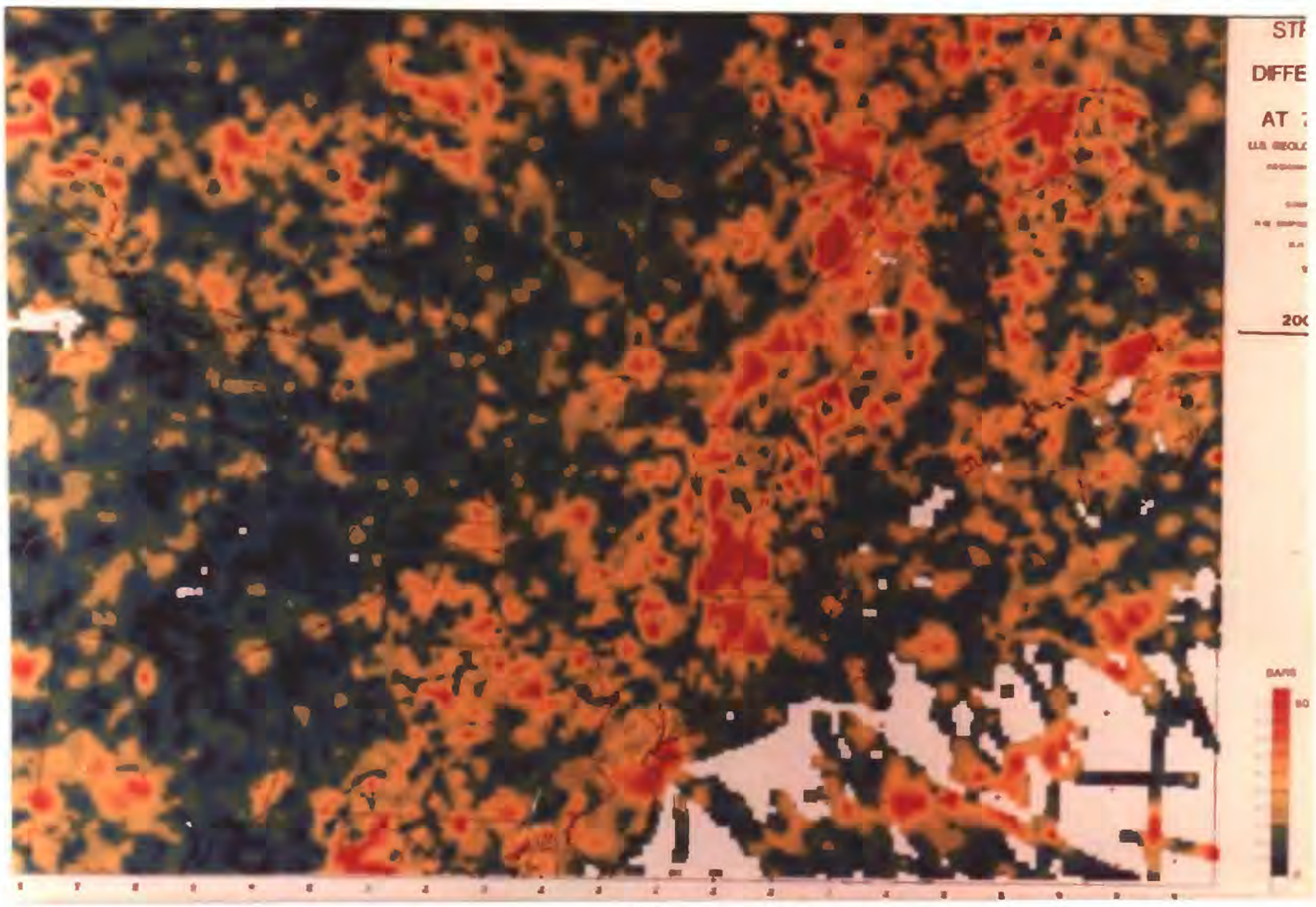

MAP 9. Terrain (range = 0 to 1550 meters)

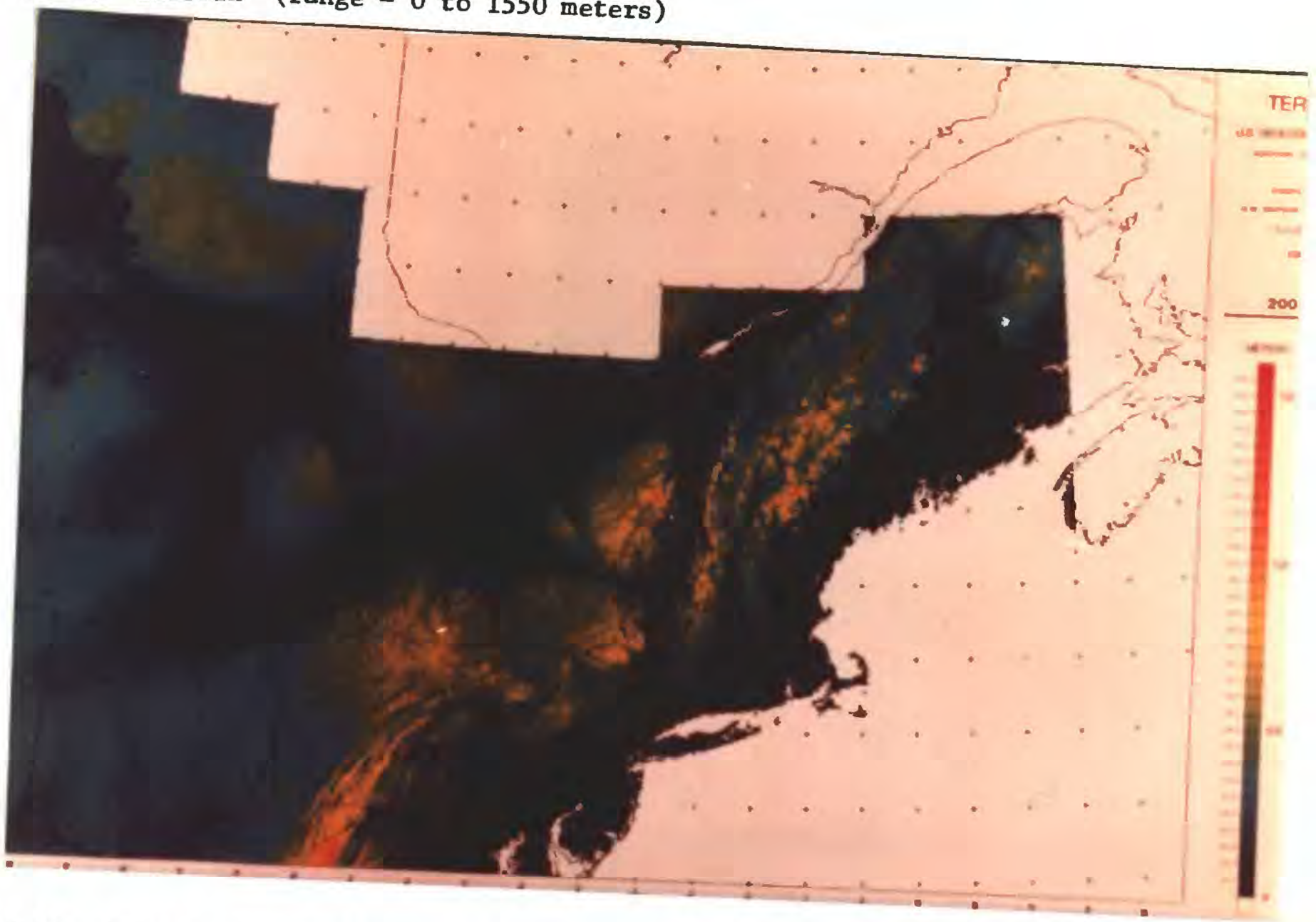

MAP 10. Terrain Slope (range = 0 to 100 meters/km)